Ellipticity control of high-order harmonic generation with nearly orthogonal two-color laser fields

Chunyang Zhai [1,*] Renzhi Shao [1,*] Pengfei Lan,[1,†] Bincheng Wang,[1] Yinfu Zhang,[1] Hua Yuan,[1]
Stephen Maina Njoroge [1] Lixin He,[1] and Peixiang Lu [1,2,‡]

[1]*Wuhan National Laboratory for Optoelectronics and School of Physics, Huazhong University of Science and Technology,
Wuhan 430074, China*
[2]*Hubei Key Laboratory of Optical Information and Pattern Recognition, Wuhan Institute of Technology, Wuhan 430205, China*

Elliptically polarized high-order harmonics opens a path toward the study of ultrafast dynamics in circular dichroism of magnetic materials, chiral molecules, and electronic spin motion. Recently, efficient high-order harmonic generation with controllable ellipticity has attracted considerable attention in experiment and theory. Here, we experimentally demonstrate a scenario using cross-linearly-polarized two-color fields consisting of a fundamental field and its second harmonic (SH). Through adjusting the relative phase, crossing angle, and intensity ratio of the cross-linearly-polarized two-color field, we obtain ellipticity-tunable high-order harmonics, with ellipticity up to $\varepsilon = 0.73$. Meanwhile, the elliptically polarized high-order harmonics preserve high efficiency. Furthermore, when the intensity of the SH field is stronger than that of the fundamental field, the even order harmonics will become several times stronger than the odd order harmonics with opposite helicity.

I. INTRODUCTION

The elliptically polarized attosecond pulses in the extreme ultraviolet (XUV) spectral range are highly desirable for applications in attosecond science and strong-field physics [1–11]. High-order harmonic generation (HHG) is a unique process to synthesize attosecond pulses. The process of HHG can be described by the semiclassical three-step model [12]; i.e., the most active electron is first freed by tunneling ionization and then accelerated in the laser field. Finally, the freed electron returns and recombines with the parent ion with emitting high-order harmonics. According to the semiclassical three-step model, the freed electron returns to the parent ion along the laser polarization direction; the high-order harmonic emission from a centrally symmetric gas medium is only linearly polarized when driven by one-color linearly polarized laser fields. When the ellipticity of the laser pulse is increased, however, the electron is driven away by the transverse field component from its parent ion so that the HHG efficiency falls off rapidly [12–16]. The ellipticity-dependent HHG efficiency is an inevitable challenge to generate bright, circularly or elliptically polarized high-order harmonics.

To produce circularly or elliptically polarized HHG [17–34] and attosecond pulses [30–38], several techniques have been proposed in the past few years. One method is based on the use of prealigned molecules [18,19]. In this approach, only a linearly polarized one-color field is required, but the measured ellipticity can hardly exceed 0.35. Alternatively, one can produce elliptically polarized HHG by modulating the driving laser. A useful method is using the bichromatic

counterrotating circularly polarized laser fields. It has been demonstrated that high-order harmonics driven by bichromatic counterrotating circularly polarized laser fields are pure circularly polarized [20–23,30–32]. And the efficiency of the high-order harmonics produced by bichromatic counterrotating circularly polarized laser fields is just slightly smaller than that with linearly polarized two-color fields [23]. However, the pairs of adjacent order harmonics appear of opposite helicity. As a result, the ellipticity of the generated attosecond pulse is still small. In recent work, noncollinear driving laser fields have also been adopted to produce elliptically polarized high-order harmonics [24,25,33,34]. One advantage of the noncollinear technique is that it offers the capability of separating the harmonics with different helicity without using a spectrometer. However, a drawback of noncollinear geometry is that it limits the interaction length over which high harmonics can be produced. In recent years, an alternative way to generate elliptically polarized high-order harmonics has also been developed based on the orthogonal two-color (OTC) fields [39,40]. By adding a weak second-harmonic (SH) field, whose intensity is about 10% of the fundamental field, to a strong fundamental field, Lambert *et al.* measured the ellipticity of high-order harmonics generated with neon [39]. Although the ellipticity of even order harmonics can reach as high as 0.75, the intensity of even order harmonics is weaker than the odd order harmonics. On the contrary, the intensity of odd order harmonics is strong, while the ellipticity of odd order harmonics is much smaller. So it is hard to synthesize a bright attosecond pulse with high degree of ellipticity.

In this paper, we experimentally demonstrate the ellipticity control of HHG by using a nearly OTC laser field (i.e., the cross-linearly-polarized two-color laser field with a big crossing angle). More importantly, compared with previous work [27], we provide experimental evidence of the important

*These authors contributed equally to this work.
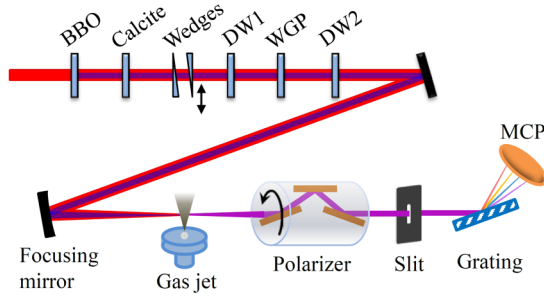†pengfeilan@hust.edu.cn
‡lupeixiang@hust.edu.cn

FIG. 1. Schematic of the experimental setup. A second harmonic is produced using a type-I BBO crystal. The group-velocity dispersion is compensated using a calcite plate. The relative phase between the SH and fundamental fields is controlled with a pair of wedges. DW1 and DW2 are dual wave plates ($\lambda/2$ at 800 nm and λ at 400 nm). WGP is a wire grid polarizer for wavelength from 250 nm to 4 μm. DW1 and WGP are used to adjust the fundamental field energy. DW2 is used to adjust the crossing angle of the polarization directions between the SH and fundamental fields. High-order harmonics are generated by focusing the two beams with a spherical mirror onto a gas jet. The polarization states of the high-order harmonics can be measured by an XUV reflective polarizer. The harmonic spectrum is recorded by an XUV spectrometer.

role of the intensity ratio besides the crossing angle in the generation process. We find that both even order and odd order harmonics will reach a very high degree of ellipticity, especially when the intensity of the SH field is comparable to or even stronger than that of the fundamental field. Furthermore, combined with the proper choice of the relative phase of the nearly OTC field, highly efficient HHG is achieved in experiment. It is worth noting that the even order harmonics present opposite helicity to the odd order harmonics, and the efficiency of even order harmonics is several times higher than that of the odd order harmonics when the SH field is stronger than the fundamental one. As a result of this selectivity, we demonstrate that the selective enhancement and helicity control of HHG can be achieved synchronously with nearly OTC fields.

II. METHOD AND EXPERIMENT

A. Experiment

In this work, we perform the experiment by using a commercial Ti:sapphire laser system (Legend Elite Duo, Coherent, Inc.). It delivers a 30-fs, 800-nm pulse at a repetition rate of 1 kHz. Figure 1 shows a schematic layout of the experiment. For the SH field generation, a β-barium borate (β-BBO) crystal (250-μm thick, type I) is used. A dual wave plate (DW1) and a wire grid polarizer (WGP) are used to continuously control the fundamental field energy. The dual wave plate is a half-wave plate for the fundamental field and a full-wave plate for the SH field. Moreover, the crossing angle θ between the polarization directions of the SH and fundamental fields is rotated by using the other dual wave plate (DW2). The time delay and the relative phase between the SH and fundamental fields are adjusted by the use of a calcite plate (2.6-mm thick) and a pair of wedges (2.8° wedge angle), respectively. By stepping one of the wedges

with a motorized stage, the relative phase between the SH and fundamental fields is controlled [41]. Since a simple and compact in-line experimental setup is used in this work, the relative phase of two-color field is stable by default. Moreover, we have compared the stability of the HHG in nearly OTC with that in the one-color field. The fluctuation of harmonic flux in the nearly OTC is similar to that in the one-color field. Therefore, the HHG stability can be assured with the compact in-line experimental setup. The relative phase between the SH and fundamental fields is determined by observing the HHG yield. The nearly OTC field is focused onto a supersonic gas jet by a spherical mirror ($f = 300$ mm). In our experiment, by adjusting both DW1 and WGP, we can selectively obtain one component of either the SH or fundamental field interacting with the gas. Then the intensities of the SH and fundamental fields are estimated by the harmonic cutoff separately when only one component interacts with the gas.

The emitted high-order harmonics are dispersed by a slit (0.1-mm wide and 15-mm high) and a flat-field grating (1200 grooves/mm). Then the high-order harmonics are imaged onto the microchannel plate (MCP) fitted with a phosphor screen. The image on the screen is finally read out by a charge-coupled device (CCD) camera [42]. The resultant high-order harmonics are polarization-analyzed with an XUV reflective polarizer comprising a rotatable triple-reflection set [23,34,43]. The triple-reflection set contains three superpolished gold-coated mirrors which reflect at about 70°-50°-70° incidence, respectively. The gold-coated mirrors have a different reflectivity for the s- and p-polarized components of the high-order harmonics [19,34,43]. With rotating the XUV reflective polarizer around the optical axis, the s- and p-polarized components change. Then one can record the intensity modulation of the high-order harmonics after passing through the XUV reflective polarizer by the XUV spectrometer [42]. Based on the Malus law, the output harmonic intensity after passing through the XUV reflective polarizer is formulated as [19,39]

$$I(\theta) = \alpha(\varepsilon)\cos(2\varphi) + c, \tag{1}$$

where α and c are two positive constants and α is a function of ε. Here φ is the rotation angle between the XUV reflective polarizer and the main polarization direction of the high-order harmonics. Figure 2 depicts the measured intensity of high-order harmonics (blue points) for different rotation angles of the XUV reflective polarizer in our experiment. To extract the polarization state of the high-order harmonics, we fit the measured harmonic intensity (red line), which follows a sine modulation, with Eq. (1). The intensity ratio between the minimum and maximum output harmonic intensity reads

$$R = \frac{I_{\min}}{I_{\max}} = \frac{R_s I_{\text{minor}} + R_p I_{\text{major}}}{R_s I_{\text{major}} + R_p I_{\text{minor}}}, \tag{2}$$

where I_{major} and I_{minor} are the intensities on the major and minor axes of the HHG ellipse, respectively. R_s and R_p are the reflectivity of the s- and p-polarized harmonics, respectively. The extinction ratio $e = R_p/R_s$ can be measured using the linearly polarized high-order harmonics generated with a linearly polarized one-color laser field. As shown in Fig. 3, the red dashed line is the measured extinction ratio e, and the blue solid line is the intensity ratio R of the high-order harmonics
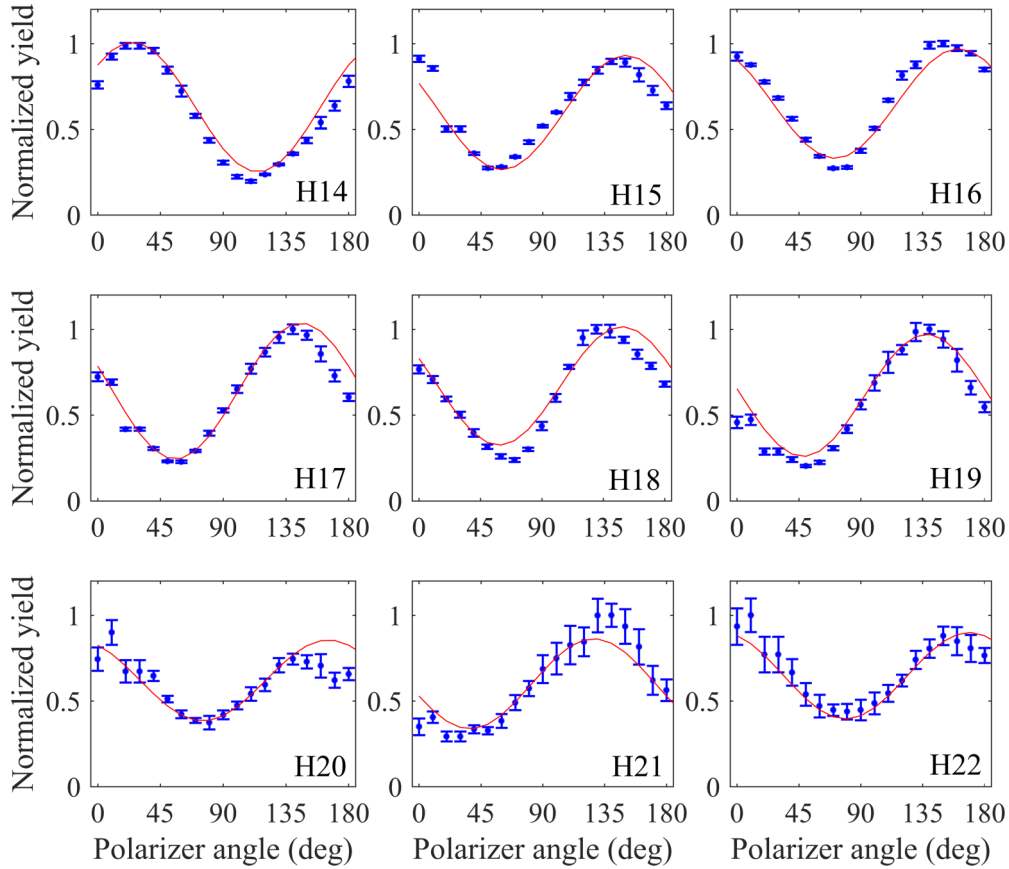
FIG. 2. High-order harmonic intensity measured as a function of the rotation angle of the XUV reflective polarizer. The blue points represent the measured data whereas the red lines represent the best fit using Eq. (1). The intensity has been normalized separately. The intensities of the SH field and the fundamental field are estimated to be 1.95×10^{14} W/cm² and 1.5×10^{14} W/cm².

shown in Fig. 2. Then the ellipticity ε of high-order harmonics can be extracted from the polarimetry measurement. It is given by

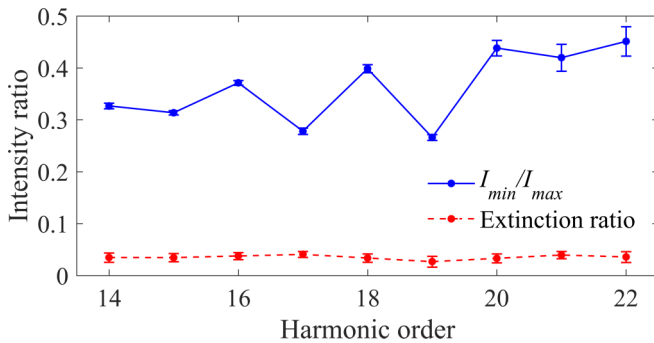$$\varepsilon = \sqrt{\frac{R - e}{1 - eR}}. \qquad (3)$$

FIG. 3. Measured ratio between the minimum and maximum of the harmonic intensity. The blue solid line displays the ratio extracted from the experimental data shown in Fig. 2. The red dashed line displays the extinction ratio extracted from the experimental data driven by a linearly polarized one-color fundamental field. The extinction ratio values of even order harmonics are averages of the adjacent odd order harmonics.

In the above method, the degree of polarization has not been considered in the measurement. In our experiment, a long pulse is used to weaken the temporal asymmetry introduced by the slow variation on the pulse edges. According to [20], a high degree of polarization (>0.9) can be achieved. On the other hand, according to [34], the decrease of the degree of polarization caused by experimental uncertainties is very weak and can be neglected. Based on these previous results [20,34], the degree of polarization will affect the ellipticity of high-order harmonics, but its influence is limited in our experiment.

B. Numerical model

To better understand the polarization properties of HHG, we theoretically calculate the high-order harmonic spectra and the ellipticity and helicity. In numerical simulation, we apply the Lewenstein model to calculate the harmonic radiation [44]. The time-dependent dipole momentum is described as (atomic units are used, unless otherwise noted) [44,45]

$$\vec{x}(t) = i \int_{-\infty}^{t} dt' \left[\frac{\pi}{\xi + i(t - t')/2} \right]^{3/2}$$
$$\times \vec{d}[\vec{p}_s(t', t) - \vec{A}(t')]\vec{d}^*[\vec{p}_s(t', t) - \vec{A}(t)]$$
$$\times e^{-iS(t', t)}\vec{E}(t')g(t') + \text{c.c.}, \qquad (4)$$

where $\vec{E}(t)$ is the laser field, $\vec{A}(t) = -\int_{-\infty}^{t} E(t')dt'$ is the corresponding vector potential, ξ is a positive regularization constant, and $\xi = 10^{-5}$ is used in our simulation. $\vec{d}[\vec{p}_s(t',t) - \vec{A}(t')]$ denotes the dipole matrix element for the photoionization transition dipole, and $\vec{d}^*[\vec{p}_s(t',t) - \vec{A}(t')]$ denotes the dipole matrix element for the photorecombination transition dipole in the length gauge. $\vec{p}_s$ and S are the stationary momentum and quasiclassical action, respectively. $g(t')$ is the ground-state probability. Then classical electrodynamics gives the harmonic spectrum as proportional to the Fourier transform of the time-dependent dipole acceleration $\vec{a}(t)$ [46],

$$\vec{\mathscr{E}}_q = \int \vec{a}(t) e^{-iq\omega t} dt. \tag{5}$$

Here, $\vec{a}(t) = \ddot{\vec{x}}(t)$. ω is the frequency of the fundamental field. q corresponds to the harmonic order. Then the harmonic intensity can be obtained by $I_q = |\vec{\mathscr{E}}_q|^2$.

The ellipticity ε of the high-order harmonic is determined by the amplitude ratio and the phase difference of the two orthogonal components,

$$\varepsilon = \tan\left(\tfrac{1}{2}\mathrm{asin}\{\sin[2\mathrm{atan}(r)]\sin(\delta)\}\right), \tag{6}$$

where the amplitude ratio $r = |\mathscr{E}_q^{\varepsilon x}|/|\mathscr{E}_q^{\varepsilon y}|$. $\mathscr{E}_q^{\varepsilon x}$ and $\mathscr{E}_q^{\varepsilon y}$ are two orthogonal components of $\vec{\mathscr{E}}_q$. δ corresponds to the phase difference between the two components.

III. RESULTS AND DISCUSSION

A. Polarization and efficiency control of high-order harmonics

Compared with one-color laser fields, two-color laser fields have more degrees of freedom, such as crossing angle, relative phase, and intensity ratio [47]. First, we measured the ellipticities of high-order harmonics generated with argon. The crossing angle θ between the polarization directions of the SH and fundamental fields is rotated from $0°$ to $90°$. Figure 4 presents the measured ellipticities of the high-order harmonics versus the crossing angle θ. One can see that although the ellipticities of some order harmonics are not increasing monotonically with crossing angle, the overall trend of the ellipticities of harmonics is an increase with the increasing of the crossing angle θ. When the crossing angle θ is above $70°$, the ellipticities of most order harmonics [especially for even orders as shown in Fig. 4(b)] become stable gradually. Subsequently, we used a nearly OTC field (fixed the crossing angle θ at $80°$) in the following work.

Then, we adjust the harmonic yield by changing the relative phase between the SH and fundamental fields. The harmonic yield appears as a periodical modulation with the changing of the relative phase of the nearly OTC field. According to the results in [48,49], we set the relative phase to 0.5π for maximizing the even harmonic yield.

Next, we investigate the influences of the laser intensity ratio $I_{2\omega}/I_\omega$ between the SH and fundamental fields. In experiment, we fixed the intensity of the fundamental field at 1.5×10^{14} W/cm^2 and scanned the intensity of the SH field. As shown in Fig. 1, the intensity of the SH field is adjusted by rotating the BBO crystal around the laser beam axis. Note that the polarization axis of the SH field is turned and the polarization state of the fundamental field is changed when
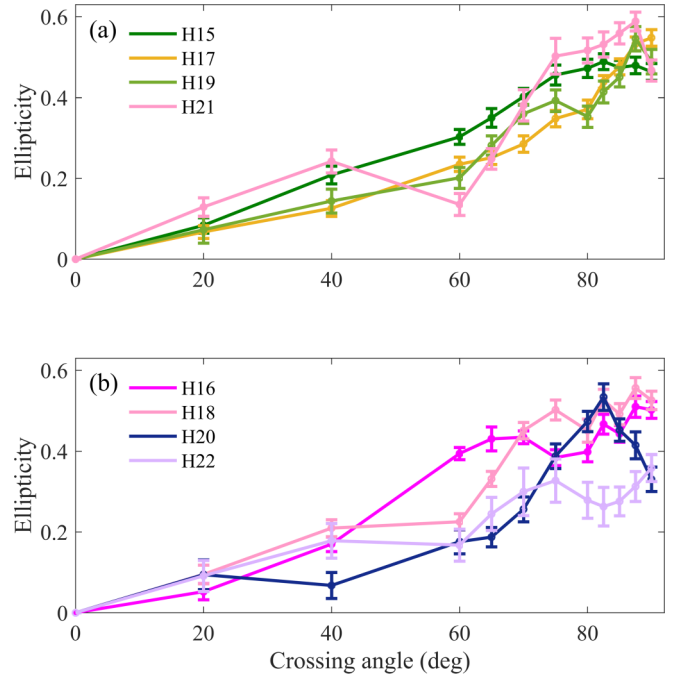

FIG. 4. Measured ellipticities for the high-order harmonics as a function of the crossing angle θ of the cross-linearly-polarized two-color laser field. The intensities of both the SH field and the fundamental field are estimated to be 1.5×10^{14} W/cm^2.

the BBO crystal is rotated. To solve this problem, we fixed the WGP's angle in the experiment to ensure that the SH and fundamental fields are both linearly polarized and parallel to each other after the WGP. The intensity of the fundamental field is fixed by adjusting the DW1. Then, one can adjust the crossing angle of the polarization directions between the SH and fundamental fields from $0°$ to $90°$ by rotating the DW2. The experimental result is shown in Fig. 5(a) with the laser intensity ratio $I_{2\omega}/I_\omega$ increasing from 0.1:1 to 1.6:1. When the SH field is weak, e.g., 10% of the fundamental field, the even order harmonics are much weaker than the odd order
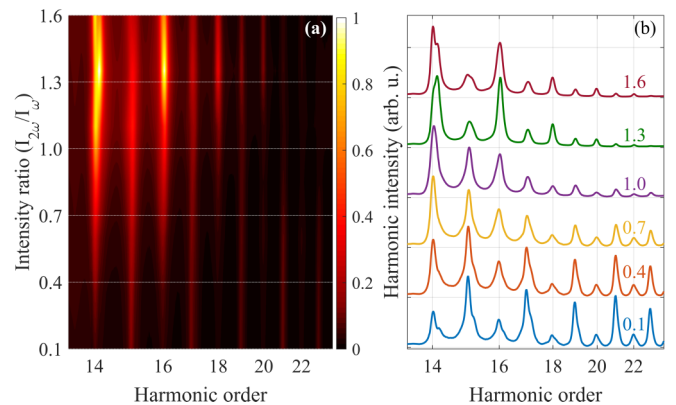

FIG. 5. (a) Measured high-order harmonics as a function of the laser intensity ratio $I_{2\omega}/I_\omega$. (b) High-order harmonic spectra for several different laser intensity ratios. High-order harmonic spectrum of each laser intensity ratio is normalized separately and shifted for clarity.
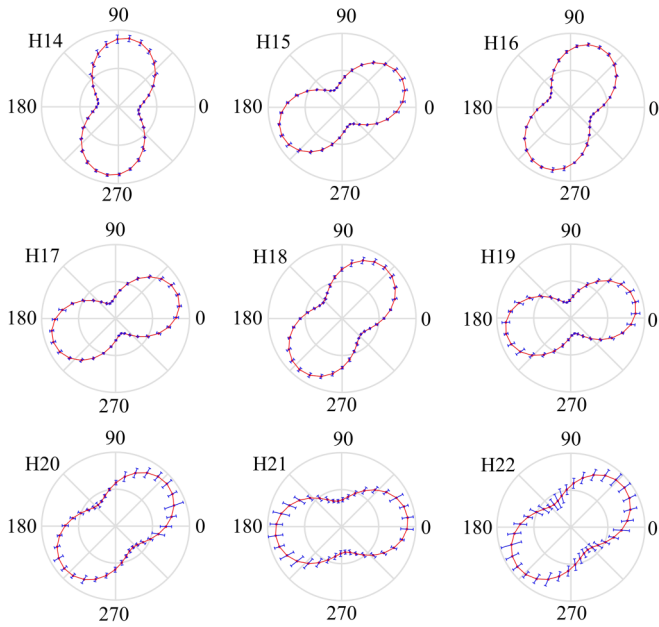
FIG. 6. The measured polarization of high-order harmonics. The intensities of the SH field and the fundamental field are estimated to be 1.95×10^{14} W/cm^2 and 1.5×10^{14} W/cm^2.
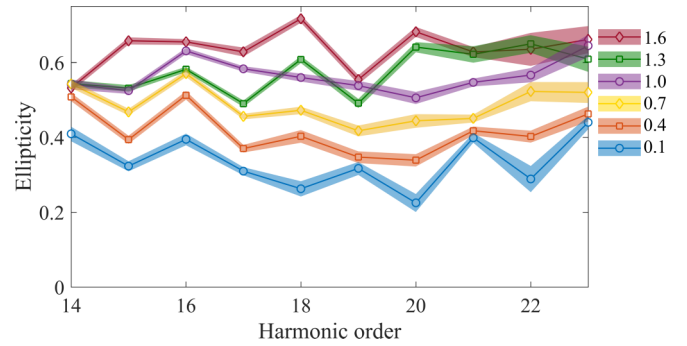

FIG. 7. The ellipticities of high-order harmonics generated in nearly OTC fields with different laser intensity ratios. The intensity of the fundamental field is fixed at 1.5×10^{14} W/cm^2, and the laser intensity ratios $I_{2\omega}/I_\omega$ are 0.1:1, 0.4:1, 0.7:1, 1.0:1, 1.3:1, and 1.6:1, respectively. The standard deviation is indicated by the width of shadows.

harmonics. This is consistent with the result in [39]. With increasing the laser intensity ratio $I_{2\omega}/I_\omega$, one can see that the intensity of the odd order harmonics is relatively stable, and contrarily, the intensity of even order harmonics increases rapidly. For the purpose of clarity, the high-order harmonic spectra are plotted in Fig. 5(b) for six values of the laser intensity ratio, and each harmonic spectrum is independently normalized. One can see that when the SH field is comparable to or even stronger than the fundamental field, the even order harmonics is stronger than the adjacent odd order harmonics. As shown in Fig. 5(a), the yield of even order harmonics reaches the maximum when the laser intensity ratio $I_{2\omega}/I_\omega$ is about 1.3:1. Then the yield of even order harmonics will decrease with further increasing of the laser intensity ratio $I_{2\omega}/I_\omega$. Note that by applying a strong SH field, the efficiency of high-order harmonics generated with OTC fields can be higher than that with the fundamental field by more than 2 orders of magnitude, and even stronger than those of the parallel polarization case [48]. The nearly OTC field is similar to the OTC field. The efficiency of the high-order harmonics generated with the bichromatic counterrotating circularly polarized laser field is slightly smaller than that with the linearly polarized two-color laser field [23]. For the noncollinear laser fields, there is a limit to the interaction length over which high-order harmonics can be produced, which could result in a reduction in harmonic flux when compared to collinear geometries [50]. Based on these previous results [23,48,50], nearly OTC fields have an advantage in terms of efficiency.

We present in Fig. 6 the polarization of the high-order harmonics with experimental data (shown in Figs. 2 and 3) driven by the nearly OTC field. The intensity of the fundamental field is estimated to be 1.5×10^{14} W/cm^2, and the intensity of the SH field is 1.3 times that of the fundamental field. From Fig. 6 it can be seen that all the harmonics from

H14 to H23 reach a high degree of elliptical polarization. Moreover, the extracted polarization axes of harmonics are shown in Fig. 6, too. One can see that the even order and odd order harmonics have different polarization directions, and this result is consistent with [27]. Figure 7 shows the measured ellipticities of high-order harmonics with different laser intensity ratio $I_{2\omega}/I_\omega$. The ellipticity ε of high-order harmonics increases from about 0.3 to 0.73 as the laser intensity ratio increases from 0.1:1 to 1.6:1. Under our experimental conditions, the higher the laser intensity ratio $I_{2\omega}/I_\omega$ is, the higher the degree of ellipticity of high-order harmonics that can be reached. For higher laser intensity ratio, it cannot be obtained in our experiment. In the simulation, we calculate higher laser intensity ratio cases and the results are shown in Fig. 8. One can see that as the laser intensity ratio increases, the ellipticities of the high-order harmonics reach a constant and then decrease [see Fig. 8(b)]. And the maximum ellipticity of lower order harmonics appears at a relatively low intensity ratio.

B. Helicity control of high-order harmonics

To give further insight into the polarization properties of HHG with nearly OTC fields, we performed the simulations using the numerical model in Sec. II B. In our simulation, to simplify the calculation, the laser field is a trapezoidal envelope with 2 optical cycles of rising and 2 optical cycles of falling edges and an 8-cycle plateau (in units of the fundamental field). The laser field intensity used in the simulation is the same as that in the experiment. We use an argon atom as the target to match the experimental conditions. Figure 9(a) represents the time-frequency distribution of the HHG with the Gabor transform. One can see that there are two harmonic radiations per optical cycle and the latter one is stronger than the former one. Note that only a short trajectory harmonic is selected with the nearly OTC field [51]. Figure 9(b) is the time-frequency distribution of the harmonic ellipticity. One can see that the harmonics radiated from two adjacent half optical cycles have opposite helicity. In the nearly OTC field scheme, the synthesized field has opposite helicity between
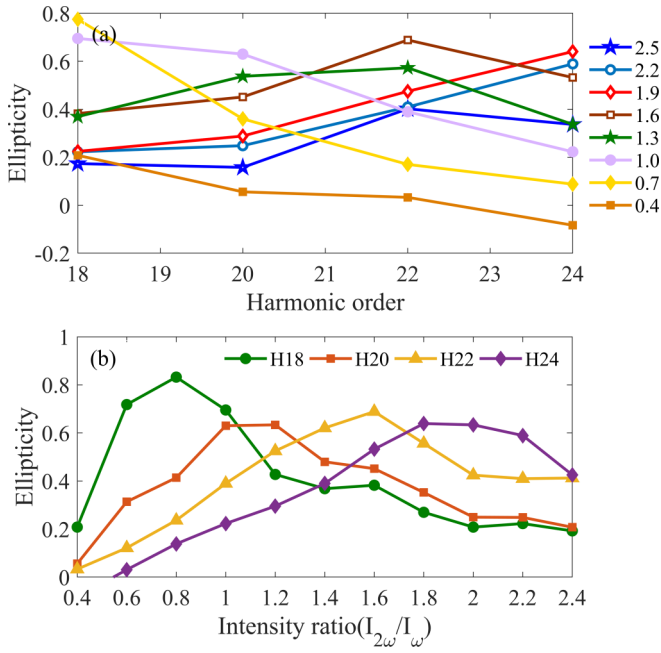
FIG. 8. Calculated ellipticities as a function of (a) harmonic order and (b) the intensity ratio $I_{2\omega}/I_{\omega}$.

two adjacent half optical cycles when its Lissajous diagram has an 8-like form [52]. The induced dipole moment d can be decomposed into d_x, which lies in the polarization direction of the fundamental field, and d_y, which lies in the direction orthogonal to that of the fundamental field. The two adjacent d_x are out of phase while the two adjacent d_y are in phase. As a result, the odd and even harmonics will exhibit opposite helicity driven by the nearly OTC field. As shown in Fig. 10(a), when the intensity of the SH field is comparable to or stronger than the fundamental field, even order and odd
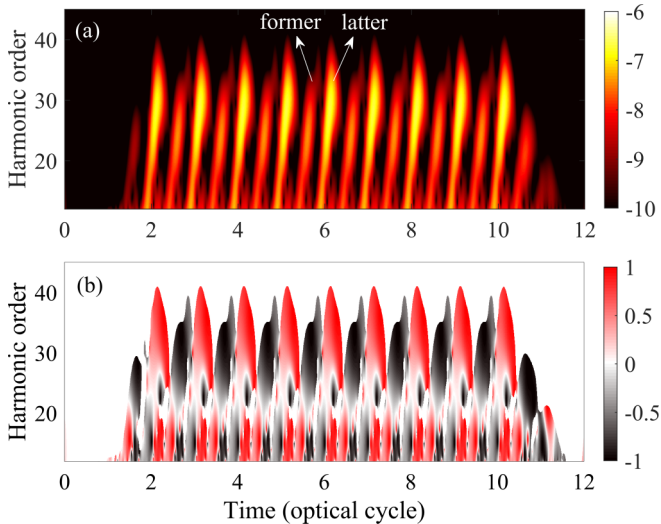

FIG. 9. (a) A time-frequency distribution of the HHG under the nearly orthogonal two-color laser field. The color map represents the time-frequency distribution in the logarithmic scale. (b) The time-frequency distribution of the harmonic ellipticity.
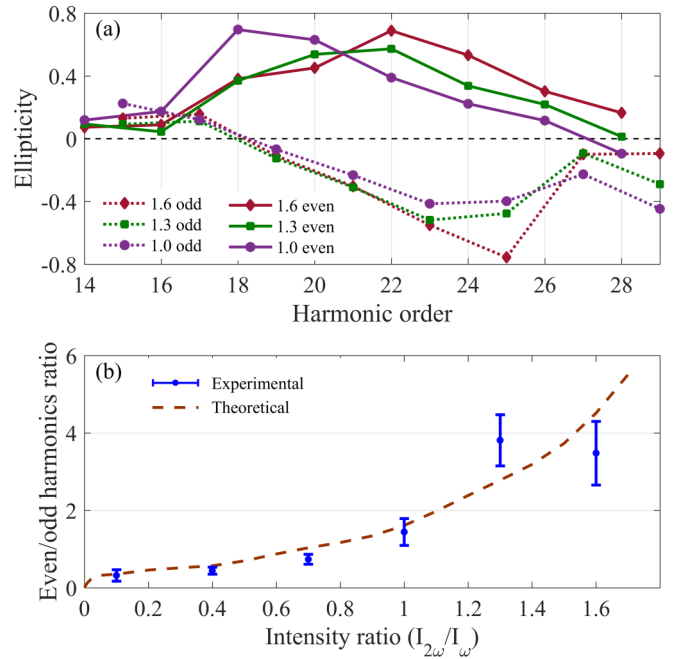

FIG. 10. (a) Simulation of the ellipticities of high-order harmonics according to the experimental conditions. The solid and dashed lines indicate even and odd order harmonics. The positive and negative ellipticities indicate that the high-order harmonics are right and left elliptically polarized. The horizontal dashed line represents the zero ellipticity. (b) Ratios between the intensities of even order and odd order harmonics. Here the intensity of even (odd) order harmonics is the sum of all the even (odd) order harmonics from H14 to H23. The blue points and brown dashed line indicate the results in experiment and simulation.

order harmonics exhibit opposite helicity in a broad frequency range. When the right elliptically polarized component (i.e., the even order harmonics) is selectively enhanced, one can produce a right elliptically polarized attosecond pulse, and vice versa. To this end, we selectively enhance the even order harmonics by adjusting the laser intensity ratio $I_{2\omega}/I_{\omega}$. Figure 10(b) presents the harmonic intensity ratio at different laser intensity ratios. One can clearly see that the harmonic intensity ratio I_{even}/I_{odd} between even order and odd order harmonics increases with increasing the laser intensity ratio $I_{2\omega}/I_{\omega}$. The intensity of the even harmonics is 4 times stronger than the odd harmonics when the laser intensity ratio $I_{2\omega}/I_{\omega}$ increases to 1.3:1. The experimental result agrees very well with the simulation. Note that through changing the laser intensity ratio of the bichromatic counterrotating circularly polarized laser field, one can selectively enhance either the left or right elliptically polarized harmonics, too. However, the change of the laser intensity ratio in favor of one color over the other will reduce the harmonic yield [30]. In contrast, the harmonic yield will increase in nearly OTC fields with increasing the intensity of the SH field.

IV. CONCLUSIONS

In conclusion, we have experimentally demonstrated that the efficiency and ellipticity of high-order harmonics can be

controlled with nearly OTC fields. On one hand, by applying a high-intensity SH field and the proper relative phase, elliptically polarized high-order harmonics are efficiently generated with the nearly OTC field. On the other hand, high-order harmonics with controllable ellipticity can be generated through adjusting the crossing angle θ and the laser intensity ratio $I_{2\omega}/I_{\omega}$. It is an effective way to adjust and control the ellipticity of high-order harmonics with nearly OTC fields, especially the intensity ratio of nearly OTC fields. When the intensity of the SH is comparable to or even stronger than the fundamental field, even and odd order harmonics exhibit opposite helicity. Notably, the intensity of even order harmonics can become several times stronger than that of odd order

harmonics. Hence, the nearly OTC field provides a possible way to generate elliptically polarized attosecond pulses.

[1] P. B. Corkum and F. Krausz, Nat. Phys. **3**, 381 (2007).

[2] F. Krausz and M. Ivanov, Rev. Mod. Phys. **81**, 163 (2009).

[3] I. Orfanos, I. Makos, I. Liontos, E. Skantzakis, B. Förg, D. Charalambidis, and P. Tzallas, APL Photonics **4**, 080901 (2019).

[4] A. D. Bandrauk, J. Guo, and K.-J. Yuan, J. Opt. **19**, 124016 (2017).

[5] F. Willems, C. T. L. Smeenk, N. Zhavoronkov, O. Kornilov, I. Radu, M. Schmidbauer, M. Hanke, C. von Korff Schmising, M. J. J. Vrakking, and S. Eisebitt, Phys. Rev. B **92**, 220405(R) (2015).

[6] G. Hu, X. Hong, K. Wang, J. Wu, H.-X. Xu, W. Zhao, W. Liu, S. Zhang, F. Garcia-Vidal, B. Wang, P. Lu, and C.-W. Qiu, Nat. Photonics **13**, 467 (2019).

[7] Á. Jiménez-Galán, G. Dixit, S. Patchkovskii, O. Smirnova, F. Morales, and M. Ivanov, Nat. Commun. **9**, 850 (2018).

[8] C. Zhai, Y. Zhang, and Q. Zhang, Opt. Commun. **437**, 104 (2019).

[9] Y. Zhao, Y. Zhou, J. Liang, Z. Zeng, Q. Ke, Y. Liu, M. Li, and P. Lu, Opt. Express **27**, 21689 (2019).

[10] T. T. Luu, M. Garg, S. Yu, A. Moulet, M. Th. Hassan, and E. Goulielmakis, Nature (London) **521**, 498 (2015).

[11] G. Vampa, T. J. Hammond, N. Thire, B. E. Schmidt, F. Legare, C. R. McDonald, T. Brabec, D. D. Klug, and P. B. Corkum, Phys. Rev. Lett. **115**, 193603 (2015); L. Li, P. Lan, L. He, W. Cao, Q. Zhang, and P. Lu, *ibid.* **124**, 157403 (2020).

[12] P. B. Corkum, Phys. Rev. Lett. **71**, 1994 (1993).

[13] K. S. Budil, P. Salieres, A. L'Huillier, T. Ditmire, and M. D. Perry, Phys. Rev. A **48**, R3437 (1993).

[14] P. Dietrich, N. H. Burnett, M. Ivanov, and P. B. Corkum, Phys. Rev. A **50**, R3585 (1994).

[15] N. H. Burnett, C. Kan, and P. B. Corkum, Phys. Rev. A **51**, R3418 (1995).

[16] S. Luo, M. Li, W. Xie, K. Liu, Y. Feng, B. Du, Y. Zhou, and P. Lu, Phys. Rev. A **99**, 053422 (2019).

[17] P.-C. Huang, C. Hernández-Garcia, J.-T. Huang, P.-Y. Huang, L. Rego, C.-H. Lu, S.-D. Yang, L. Plaja, A. H. Kung, and M.-C. Chen, IEEE J. Sel. Top. Quant. **25**, 1 (2019).

[18] J. Levesque, Y. Mairesse, N. Dudovich, H. Pépin, J. C. Kieffer, P. B. Corkum, and D. M. Villeneuve, Phys. Rev. Lett. **99**, 243001 (2007).

[19] X. Zhou, R. Lock, N. Wagner, W. Li, H. C. Kapteyn, and M. M. Murnane, Phys. Rev. Lett. **102**, 073902 (2009).

[20] L. Barreau, K. Veyrinas, V. Gruson, S. J. Weber, T. Auguste, J. F. Hergott, F. Lepetit, B. Carré, J. C. Houver, D. Dowek, and P. Salières, Nat. Commun. **9**, 4727 (2018).

[21] O. Kfir, P. Grychtol, E. Turgut, R. Knut, D. Zusin, D. Popmintchev, T. Popmintchev, H. Nembach, J. M. Shaw, A. Fleischer, H. Kapteyn, M. Murnane, and O. Cohen, Nat. Photonics **9**, 99 (2014).

[22] T. Fan, P. Grychtol, R. Knut, C. Hernández-Garcia, D. D. Hickstein, D. Zusin, C. Gentry, F. J. Dollar, C. A. Mancuso, C. W. Hogle, O. Kfir, D. Legut, K. Carva, J. L. Ellis, K. M. Dorney, C. Chen, O. G. Shpyrko, E. E. Fullerton, O. Cohen, P. M. Oppeneer, D. B. Milošević, A. Becker, A. A. Jaroń-Becker, T. Popmintchev, M. M. Murnane, and H. C. Kapteyn, Proc. Natl. Acad. Sci. USA **112**, 14206 (2015).

[23] A. Fleischer, O. Kfir, T. Diskin, P. Sidorenko, and O. Cohen, Nat. Photonics **8**, 543 (2014); Q. Ke, Y. Zhou, J. Tan, M. He, J. Liang, Y. Zhao, M. Li, and P. Lu, Opt. Express **27**, 32193 (2019).

[24] D. D. Hickstein, F. J. Dollar, P. Grychtol, J. L. Ellis, R. Knut, C. Hernández-García, D. Zusin, C. Gentry, J. M. Shaw, T. Fan, K. M. Dorney, A. Becker, A. Jaroń-Becker, H. C. Kapteyn, M. M. Murnane, and C. G. Durfee, Nat. Photonics **9**, 743 (2015).

[25] J. L. Ellis, K. M. Dorney, D. D. Hickstein, N. J. Brooks, C. Gentry, C. Hernandez-Garcia, D. Zusin, J. M. Shaw, Q. L. Nguyen, C. A. Mancuso, G. S. M. Jansen, S. Witte, H. C. Kapteyn, and M. M. Murnane, Optica **5**, 479 (2018).

[26] Z. Y. Chen and A. Pukhov, Nat. Commun. **7**, 12515 (2016).

[27] B. Mahieu, S. Stremoukhov, D. Gauthier, C. Spezzani, C. Alves, B. Vodungbo, P. Zeitoun, V. Malka, G. De Ninno, and G. Lambert, Phys. Rev. A **97**, 043857 (2018).

[28] D. Azoury, O. Kneller, M. Krüger, B. D. Bruner, O. Cohen, Y. Mairesse, and N. Dudovich, Nat. Photonics **13**, 198 (2019).

[29] F. Kong, C. Zhang, H. Larocque, Z. Li, F. Bouchard, D. H. Ko, G. G. Brown, A. Korobenko, T. J. Hammond, R. W. Boyd, E. Karimi, and P. B. Corkum, Nat. Commun. **10**, 2020 (2019).

[30] K. M. Dorney, J. L. Ellis, C. Hernández-Garcia, D. D. Hickstein, C. A. Mancuso, N. Brooks, T. Fan, G. Fan, D. Zusin, C. Gentry, P. Grychtol, H. C. Kapteyn, and M. M. Murnane, Phys. Rev. Lett. **119**, 063201 (2017).

[31] L. Medišauskas, J. Wragg, H. van der Hart, and M. Y. Ivanov, Phys. Rev. Lett. **115**, 153001 (2015).

[32] N. Zhavoronkov and M. Ivanov, Opt. Lett. **42**, 4720 (2017).

[33] C. Hernández-García, C. G. Durfee, D. D. Hickstein, T. Popmintchev, A. Meier, M. M. Murnane, H. C. Kapteyn, I. J. Sola, A. Jaron-Becker, and A. Becker, Phys. Rev. A **93**, 043855 (2016).

[34] P. C. Huang, C. Hernández-García, J. T. Huang, P. Y. Huang, C. H. Lu, L. Rego, D. D. Hickstein, J. L. Ellis, A. Jaron-Becker, A. Becker, S. D. Yang, C. G. Durfee, L. Plaja, H. C. Kapteyn, M. M. Murnane, A. H. Kung, and M. C. Chen, Nat. Photonics **12**, 349 (2018).

[35] C. Chen, Z. Tao, C. Hernández-García, P. Matyba, A. Carr, R. Knut, O. Kfir, D. Zusin, C. Gentry, P. Grychtol, O. Cohen, L. Plaja, A. Becker, A. Jaron-Becker, H. Kapteyn, and M. Murnane, Sci. Adv. **2**, e1501333 (2016).

[36] O. Kfir, P. Grychtol, E. Turgut, R. Knut, D. Zusin, A. Fleischer, E. Bordo, T. Fan, D. Popmintchev, T. Popmintchev, H. Kapteyn, M. Murnane, and O. Cohen, J. Phys. B: At., Mol. Opt. Phys. **49**, 123501 (2016).

[37] K. M. Dorney, L. Rego, N. J. Brooks, J. Román, C.-T. Liao, J. L. Ellis, D. Zusin, C. Gentry, Q. L. Nguyen, J. M. Shaw, A. Picón, L. Plaja, H. C. Kapteyn, M. M. Murnane, and C. Hernández-García, Nat. Photonics **13**, 123 (2019).

[38] K. Mi, W. Cao, H. Xu, Y. Mo, Z. Yang, P. Lan, Q. Zhang, and P. Lu, Phys. Rev. Appl. **13**, 014032 (2020); Z. Yang, W. Cao, X. Chen, J. Zhang, Y. Mo, H. Xu, K. Mi, Q. Zhang, P. Lan, and P. Lu, Opt. Lett. **45**, 567 (2020).

[39] G. Lambert, B. Vodungbo, J. Gautier, B. Mahieu, V. Malka, S. Sebban, P. Zeitoun, J. Luning, J. Perron, A. Andreev, S. Stremoukhov, F. Ardana-Lamas, A. Dax, C. P. Hauri, A. Sardinha, and M. Fajardo, Nat. Commun. **6**, 6167 (2015).

[40] S. Stremoukhov, A. Andreev, B. Vodungbo, P. Salières, B. Mahieu, and G. Lambert, Phys. Rev. A **94**, 013855 (2016).

[41] C. Zhai, X. Zhang, X. Zhu, L. He, Y. Zhang, B. Wang, Q. Zhang, P. Lan, and P. Lu, Opt. Express **26**, 2775 (2018).

[42] B. Wang, L. He, Y. He, Y. Zhang, R. Shao, P. Lan, and P. Lu, Opt. Express **27**, 30172 (2019).

[43] T. Hahn, J. Bierbach, C. Rödel, D. Hemmers, M. Yeung, B. Dromey, S. Fuchs, A. Galestian, S. Kuschel, M. Zepf, G. G. Paulus, and G. Pretzler, Appl. Phys. B: Lasers Opt. **118**, 241 (2015).

[44] M. Lewenstein, P. Balcou, M. Y. Ivanov, A. L'Huillier, and P. B. Corkum, Phys. Rev. A **49**, 2117 (1994).

[45] P. Antoine, B. Carré, A. L'Huillier, and M. Lewenstein, Phys. Rev. A **55**, 1314 (1997).

[46] J. D. Jackson, *Classical Electrodynamics*, 2nd ed. (Wiley, New York, 1975), p. 658.

[47] A. V. Andreev, S. Stremoukhov, and O. A. Shoutova, J. Opt. Soc. Am. B **30**, 1794 (2013).

[48] I. J. Kim, C. M. Kim, H. T. Kim, G. H. Lee, Y. S. Lee, J. Y. Park, D. J. Cho, and C. H. Nam, Phys. Rev. Lett. **94**, 243901 (2005).

[49] H. Yun, K. M. Lee, J. H. Sung, K. T. Kim, H. T. Kim, and C. H. Nam, Phys. Rev. Lett. **114**, 153901 (2015).

[50] J. L. Ellis, K. M. Dorney, C. G. Durfee, C. Hernández-García, F. Dollar, C. A. Mancuso, T. Fan, D. Zusin, C. Gentry, P. Grychtol, H. C. Kapteyn, M. M. Murnane, and D. D. Hickstein, Opt. Express **25**, 10126 (2017).

[51] C. M. Kim and C. H. Nam, J. Phys. B: At., Mol. Opt. Phys. **39**, 3199 (2006).

[52] P. V. Demekhin, A. N. Artemyev, A. Kastner, and T. Baumert, Phys. Rev. Lett. **121**, 253201 (2018).